

PoI: Pixel of Interest for Novel View Synthesis Assisted Scene Coordinate Regression

Feifei Li¹, Qi Song², Chi Zhang³, Hui Shuai⁴ and Rui Huang⁵

{feifeili1, qisong, chizhang1}@link.cuhk.edu.cn, huishuai13@163.com, ruihuang@cuhk.edu.cn

Abstract

The task of estimating camera poses can be enhanced through novel view synthesis techniques such as NeRF and Gaussian Splatting to increase the diversity and extension of training data. However, these techniques often produce rendered images with issues like blurring and ghosting, which compromise their reliability. These issues become particularly pronounced for Scene Coordinate Regression (SCR) methods, which estimate 3D coordinates at the pixel level. To mitigate the problems associated with unreliable rendered images, we introduce a novel filtering approach, which selectively extracts well-rendered pixels while discarding the inferior ones. This filter simultaneously measures the SCR model’s real-time reprojection loss and gradient during training. Building on this filtering technique, we also develop a new strategy to improve scene coordinate regression using sparse inputs, drawing on successful applications of sparse input techniques in novel view synthesis. Our experimental results validate the effectiveness of our method, demonstrating state-of-the-art performance on indoor and outdoor datasets.

1 Introduction

Visual localization, also known as camera relocalization, is a fundamental task in computer vision that involves estimating the 6-degree-of-freedom (6DOF) camera poses within a known scene based on input images. This task plays a crucial role in Simultaneous Localization and Mapping (SLAM) Izadi *et al.* [2011]; Mur-Artal *et al.* [2015]; Dai *et al.* [2017]; Tang and Tan [2018] and has significant applications in areas such as autonomous driving, robotics, and virtual reality.

Learning-based methods for camera relocalization can be categorized into two main types: Camera Pose Regression (CPR) methods Purkait *et al.* [2018]; Chen *et al.* [2021]; Ng *et al.* [2021]; Taira *et al.* [2018]; Moreau *et al.* [2022a,b]; Chen *et al.* [2022] and Scene Coordinate Regression (SCR) methods Brachmann and Rother [2021]; Brachmann *et al.* [2017]; Brachmann and Rother [2019]; Shotton *et al.* [2013]; Valentin *et al.* [2015]; Brachmann *et al.* [2023]. Between these, SCR

frameworks are particularly favored due to their higher accuracy. However, both approaches require stringent sampling density of training data to ensure reliable pose estimations for arbitrary images captured within a specific scene. Manually collecting a sufficient number of training images is a time-consuming process, and obtaining the corresponding camera pose labels presents further difficulties.

In light of this, some CPR-based methods try to enrich the training set with synthetic data rendered by novel view synthesis (NVS) techniques. For example, LENS Moreau *et al.* [2022b] employs NeRF to render views of average sampled novel poses, thereby augmenting the training dataset and treating these synthetic images similarly to real data without additional processing. Similarly, DFNet Chen *et al.* [2022] utilizes NeRF-W Martin-Brualla *et al.* [2021] for NVS and features a cross-domain design that helps to minimize the discrepancies between synthetic and query images, effectively bridging the gap between the two domains.

Currently, there is no similar research within the SCR framework, and we raise the question of whether SCR-based pipelines can also benefit from synthetic images. To this end, we attempt to apply NVS for data augmentation within the SCR framework. However, we found that SCR methods, which rely on precise pixel-to-pixel (N2N) predictions, are particularly vulnerable to the quality of rendered images. This contrasts with CPR methods, which involve pixel-to-pose predictions and are less affected by image quality. As shown in the right section of Figure 1, after expanding the training dataset with synthetic data through NVS, the CPR method shows significant improvement, while SCR performance declines, accompanied by a notable increase in training time. Directly training the SCR model with raw rendered images proves less effective than CPR methods and may even result in model collapse if the proportion of rendered images is excessively high.

To address this issue, we designed a portable pixel of interest (PoI) module that serves as an effective filter for synthetic clues. Specifically, the 3D-to-2D projection error of each pixel is employed as a criterion for whether the point is retained or not, and a rough to precise threshold setting is used for screening at different training stages. As the training progresses, PoI gradually removes poorly rendered pixels and further leverages the remaining points alongside real data to train the network.

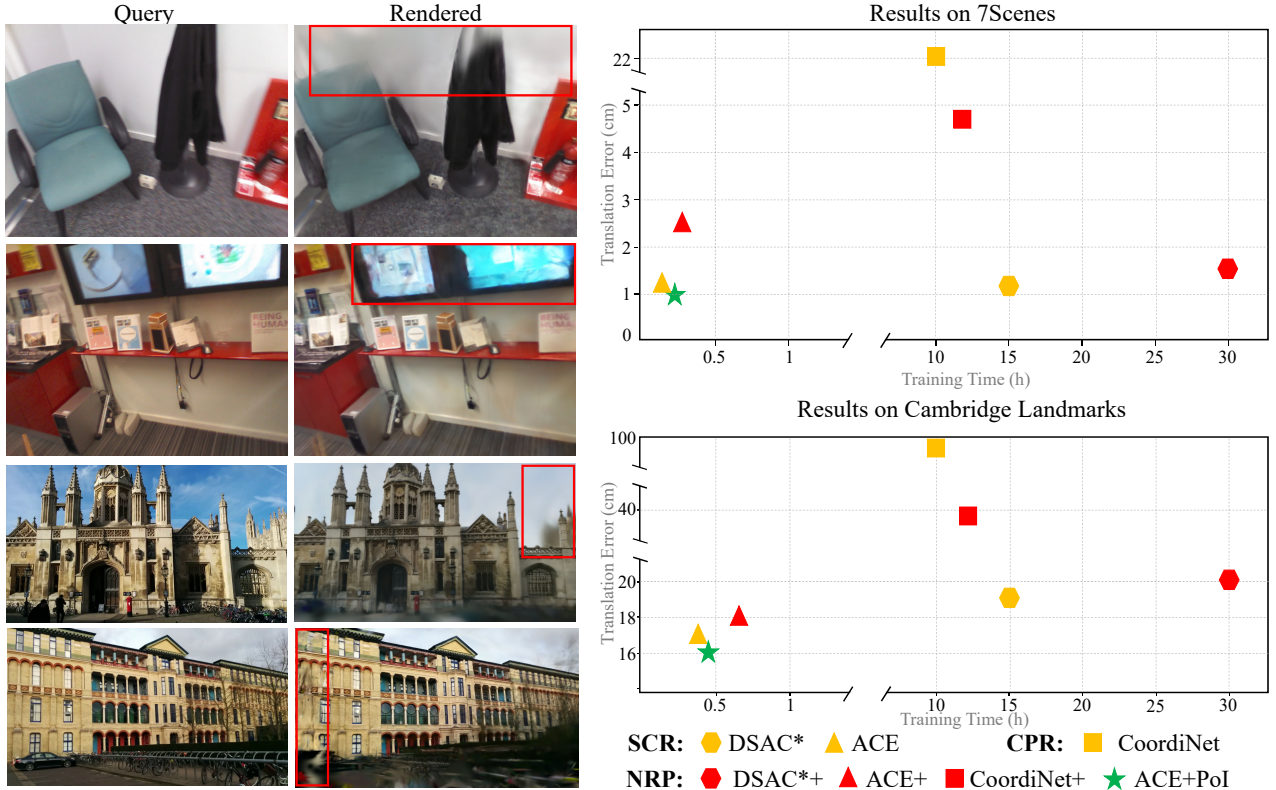


Figure 1: **Left:** Comparison of query and rendered images of the dataset 7Scenes and Cambridge Landmarks, revealing uneven rendering quality within frames, with some parts clear and others blurry or ghosted; **Right:** Translation error versus training time, where "CoordiNet" means using rendered images as query images for CPR method CoordiNet (LENS in this case); "DSAC*+" and "ACE+" denote the method combines NVS-rendered images and query images as training data for SCR method DSAC* and ACE. "ACE+PoI" denotes our method PoI (ACE-based); We can see that directly adding rendered data to the training set will increase training time to some extent, but performance will decrease for the SCR method. On the other hand, our PoI approach can improve the performance with an acceptable time increase.

Moreover, we propose a coarse-to-fine variant of PoI to address the challenges of visual localization in extreme scenarios, especially where the amount of training data is limited. In the coarse stage, we receive all available synthetic data as input and gradually train a coarse model by self-pruning to remove noisy pixels. Following this, we fine-tune the coarse model using sparse real pixels. This method enables our PoI variant to efficiently leverage sparse input while ensuring strong pose estimation performance, even under difficult conditions.

The main contributions of our work are summarized as follows:

- We introduce PoI, a pixel-level filter designed to eliminate poorly rendered pixels for effective training data augmentation.
- We present an innovative approach to tackle scene coordinate regression from sparse inputs.
- Our method achieves state-of-the-art performance on both indoor and outdoor datasets.

2 Related Work

Camera Pose Regression The CPR methods, i.e., to regress the camera pose from the given image directly, are the most naive ideas and most widely used in learning-based methods Kendall *et al.* [2015]; Brachmann *et al.* [2016]; Brahmbhatt *et al.* [2018]; Melekhov *et al.* [2017]; Radwan *et al.* [2018]; Wang *et al.* [2020]; Hu *et al.* [2020]; Arnold *et al.* [2022]; Chen *et al.* [2022]; Shavit and Keller [2022]. The most straightforward method implicitly uses CNN layers or MLP to represent the image-to-pose correspondence. PoseNet Kendall *et al.* [2015] first proposes this using pre-trained GoogLeNet as the feature extractor. Then, several works focus on improving CPR through additional modules. Geomapnet Brahmbhatt *et al.* [2018] estimates the absolute camera poses and the relative poses between adjacent frames. AtLoc Wang *et al.* [2020] uses a self-attention module to extract salient features from the image. Vlocnet++ Radwan *et al.* [2018] adds a semantic module to solve the dynamic scene and improve the robustness for blockings and blurs. Marepo Chen *et al.* [2024a] first regresses the scene-specific geometry from the input images and then estimates the camera pose using a scene-agnostic transformer. The CPR method has achieved excellent efficiency and simplification

of the framework, but there is still room for improvement in accuracy.

Scene Coordinate Regression Recently, the SCR methods Shotton *et al.* [2013]; Brachmann *et al.* [2017]; Brachmann and Rother [2018, 2019]; Massiceti *et al.* [2017]; Li *et al.* [2018]; Brachmann and Rother [2021]; Liu *et al.* [2025] have achieved better performance in terms of the accuracy compared with the CPR methods. The SCR method aims to estimate the coordinates of the points in 3D scenes instead of relying on the feature extractor to find salient descriptors, as in CPR methods. SCR was initially proposed using the random forest for RGB-D images Shotton *et al.* [2013]. Recently, estimating scene coordinates through RGB input has been widely studied. ForestNetMassiceti *et al.* [2017] compares the benefits of Random Forest (RF) and Neural Networks in evaluating the scene coordinate and camera poses. ForestNet also proposes a novel method to initiate the neural network from an RF. DSAC Brachmann *et al.* [2017], DSAC++ Brachmann and Rother [2018] devise a differentiable RANSAC, and thus the SCR method can be trained end-to-end. ESAC Brachmann and Rother [2019] uses a mixture of expert models (i.e., a gating network) to decide which domain the query belongs to, and then the complex SCR task can be split into simpler ones. DSAC* Brachmann and Rother [2021] extends the previous works to applications using RGB-D or RGB images, with/without the 3D models. This means that in the minimal case, only RGB images will be used as the input to DSAC*, just like most CPR methods. More information about the 3D structure will be utilized for most SCR methods than CPR ones. However, approaches like DSAC* can achieve more accurate estimations even if the input is the same as the CPR method. ACE Brachmann *et al.* [2023] and GLACE Wang *et al.* [2024] abandon the time-consuming end-to-end supervision module and shuffle all pixels of the scene to improve training efficiency. ACE and GLACE use only RGBs without extra 3D geometry information and achieve comparable accuracy compared with former methods.

Despite the progress of CPR and SCR methods, both methods still have great problems in data collection and labeling. Therefore, efficient data collection and labeling methods or alternatives with similar effects are needed.

Neural render pose estimation (NRP) A major challenge for visual localization methods is to collect appropriate photos to cover the entire scene. Essentially, the number and distribution of image sets for training are difficult to decide. For example, most outdoor scenes collect data along roads, such as Cambridge landmarks Kendall *et al.* [2015]. For indoor datasets (such as the 7Scenes Shotton *et al.* [2013] dataset), all translations and orientations within the scene are considered.

To fulfill the diverse requirements of data collection, some works try to use more flexible NVS to render synthetic views instead of collecting extra data Chen *et al.* [2021]; Ng *et al.* [2021]; Purkait *et al.* [2018]; Taira *et al.* [2018]; Moreau *et al.* [2022b]; Chen *et al.* [2022], where NVS is the method to render synthetic images from the camera poses, which can verify the accuracy of 3D reconstruction, especially for implicit reconstruction methods like NeRF Mildenhall *et al.*

[2021], and 3DGS Kerbl *et al.* [2023]. INeRF Yen-Chen *et al.* [2021] applies an inverted NeRF to optimize the estimated pose through color residual between rendered and observed images. However, the initially estimated poses are significant in guaranteeing the convergence of outputs. LENS Moreau *et al.* [2022b] samples the poses uniformly throughout the area and trains a NeRF-W Martin-Brualla *et al.* [2021] to render the synthetic images. Then, rendered images and poses work as the additional training data for the pose regression network. The limitation of LENS lies in the costly offline computation for dense samples. DFNet uses direct feature matching between observed and synthetic images generated by histogram-assisted NeRF. The feature match approach is proposed to extract observed or generated images' cross-domain information. All these methods combine the NVS module and the CPR module to optimize the performance of the absolute pose estimation of the photos.

Unlike the former methods, we propose using an SCR rather than the CPR method with proposed NVS rules to improve the camera pose estimation. First, we design novel pose sampling methods to meet multiple requirements of different datasets. To address the problem of varying lighting conditions, we use exposure histogram-assisted 3DGS as the baseline to sample new views of multiple exposures for each sampled pose in outdoor datasets. Second, we propose a pixel filter to remove bad pixels in rendered images and use query frames and remaining rendered pixels to improve the estimation.

3 Method

In general, the pipeline of our proposed method is shown in Figure 2. For the input query images I_q , and corresponding camera poses P_q , we first sample the novel camera pose P_n using Grid Sampling (GS). Then we render novel views I_n using 3DGS. Finally, we use PoI to estimate the scene coordinates through the input I_q, I_n . During test time, we use PNP-based Ransac to infer the camera poses from the scene coordinates.

The following part of this chapter is arranged as follows:

- Chapter 3.2 elaborates on the pipeline of the proposed method: PoI;
- Chapter 3.3 explains the filtering strategy of PoI.
- Chapter 3.4 describes the applicable conditions and limitations of using PoI as a plugin.
- Chapter 3.5 explains the variant of PoI in extreme cases of sparse input.

3.1 NVS models used in our approach

This paper uses 3DGS Kerbl *et al.* [2023] as the baseline for novel view synthesis. A big challenge in NVS is the change in illumination conditions. The same situation also exists in the localization problem. To tackle this problem, We apply the luminance histogram method from DFNet Chen *et al.* [2022] to adjust the appearance of the rendering images in 3DGS. we generate the exposure embedding from the luminance histogram and output the affine transformation from an MLP used in wild Gaussians Kulhanek *et al.* [2024].

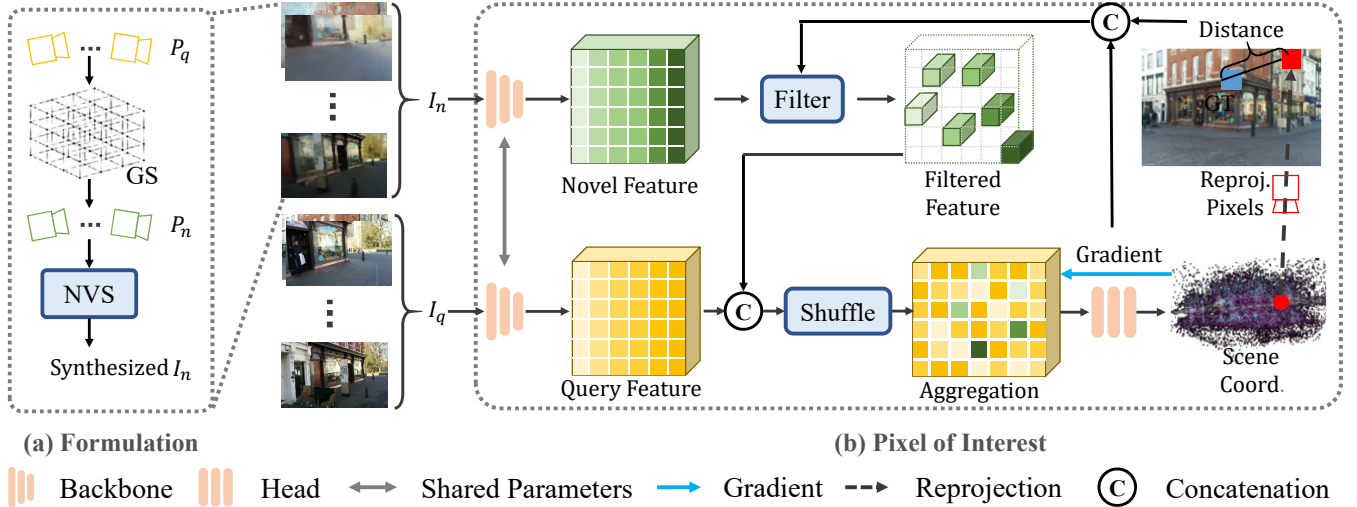


Figure 2: Pipeline of our proposed methods: **(a) data formulation**: We first sample a group of synthesized camera poses P_n according to the query training pose P_q using ‘GS’ (grid sampling). Then, we render the synthesized views I_n based on the sampled poses P_n through the novel view synthesis model. **(b) architecture of PoI**: First, a pre-trained scene-irrelevant backbone is applied to extract the features of the input query photos I_q and the synthesized novel images I_n . Then, the filter is applied to the features of the rendered images and gets the features of interest. After that, we combine the query features with the filtered novel features and shuffle the pixel-aligned features to get the aggregation. Finally, we estimate the scene coordinates of the pixels using a scene-specific Head. The filtering algorithm is designed based on the reprojection error of the estimated scene coordinates.

3.2 Pixel of interest (PoI)

In order to use rendered images as the auxiliary input for camera pose estimation, most existing methods estimate the scene coordinates of all pixels (or downsampled pixels) of the rendered image without considering the differences in the rendering quality of these pixels, which greatly increases the time and resource cost of training and reduces the effectiveness of the auxiliary data. To improve efficiency and robustness, we consider reducing the number of rendered pixels compared to query images for training. Since the 3DGS-based reconstruction method predicts the target RGB pixel-wise without cross-pixel guidance, the rendering quality of different pixels from the same image would be independent. So, if we reduce the rendered images frame-wise, some well-rendered pixels of the discarded images would also be removed. To address this problem, we propose a method that finds the well-rendered pixels of the frame: pixels of interest.

The architecture of PoI is shown in Figure 2.(b). In order to rule out pixels with poor rendering effects, we need a method to obtain pixel-level feature supervision instead of frame-level feature map supervision. To this end, we use the pre-trained scene-independent convolutional network from Ace Brachmann *et al.* [2023] as our backbone to obtain frame-level feature maps, and we will freeze the parameters of this backbone network throughout the training process. We input the query images I_q and the synthesized images I_n into the backbone to obtain the query features and novel features. We keep all the query features while using a filtering algorithm to extract features of interest (FoI) from the novel features.

3.3 Filtering strategy

The filtering process can be divided into two parts: First, we randomly sample the novel features in a specific ratio. We want to use more features from query images and fewer features from rendered images to avoid the collapse of the model caused by low-quality rendered pixels, so we set the ratio to 0.5 in our experiments; this ratio is related to the performance of NVS; we may choose a bigger ratio with a better NVS method. This can also be solved through different novel pose sampling methods. Second, the filtering threshold is set based on the joint metric of gradient and training loss. For faster convergence, we use a pseudo-depth strategy for poorly performing pixels. When the reprojection error of a point exceeds a certain threshold, we first let these points converge to the target pseudo-depth. After that, these pixels are trained normally as the others. Because we should also find PoI in the same stage, gradient alone cannot represent rendering quality in this case. we should also use reprojection error (the distance between GT planar coordinates and estimated re-projected planar coordinates) for filtering. Therefore, pixels with smaller gradients and lower reprojection loss are retained.

We implement filtering operations at the intermediate stage of training. The filter will remove novel features of outlier prediction. The remaining features are the so-called FoI, and the corresponding pixels of FoI are the so-called PoI. Figure 3 shows an example of the PoI results in the 7Scenes and Cambridge Landmarks datasets. After filtering, we combine and shuffle the features F and FoI and put them into the scene-specific MLP Head to estimate the scene coordinates.

It is worth mentioning that we have set a dynamic weight for the loss of rendering pixels. Because in the early stage of

training, we want the model to converge quickly. After determining the PoI, we gradually reduce the weight of the loss of PoI from 1 to 0.01, while for the pixels from query images, we set the weight to 1 during the entire training process.

$$\begin{aligned} \mathcal{L} &= \begin{cases} \mathcal{L}_{rep}^{query}(i), & \text{if } i \in T \\ \tilde{\omega} \times \mathcal{L}_{rep}^{poi}(i), & \text{if } i \in PoI \end{cases} \\ \tilde{\omega} &= \omega_{max} - \frac{I_{iter}}{N_{iter}}(\omega_{max} - \omega_{min}) \end{aligned} \quad (1)$$

where T denotes training data, $\tilde{\omega}$ denotes the dynamic weight of PoI loss changing from ω_{max} (set 1) to ω_{min} (set 0.01). I_{iter} denotes the current iteration number and N_{iter} is the total iterations. All rendering data is initially set as PoI. As the training progresses, we rule out outlier prediction points from PoI. At the end of the training, the choice of PoI and the loss weight of PoI are fixed.

In PoI, we would sample novel camera poses and render the corresponding images according to the images and the corresponding camera poses from the training set. In existing novel view synthesis supported visual localization, we usually have to balance the novel poses' diversity and the images' overall rendering quality. However, we do not need an overall well-rendered image in the PoI task because of the pixel-level optimization and filtering algorithm. Therefore, we should try to expand the diversity of novel poses. We use a unified sampling method for camera pose translation: grid sampling. The boundaries of the grid are calculated based on the camera pose of the training data; that is, the maximum and minimum values of the grid (x, y, z) are determined by the maximum and minimum values of the translations of all camera poses. We add a random perturbation to the rotation. The original rotation of each grid starts from the closest camera pose to that grid in the training data.

3.4 Applicable conditions and limitations

For the end-to-end SCR approach, PoI is difficult to use as a plug-and-play module, which is the limitation of the PoI method. First, end-to-end SCR methods use image-level loss as a supervision and have no pixel-level performance, which makes PoI unusable in these methods. Furthermore, even for two-stage SCR methods (init+e2e) such as DSAC*, all pixels of the same image should be supervised within one iteration in the e2e stage. If we filter out some pixels of the rendered images, aligning the rendered features and designing a differentiable RANSAC algorithm is difficult. Finally, pixel-wise shuffling (which is difficult to achieve in e2e) is also an important factor; without shuffling, poorly rendered pixels are more likely to appear in a batch of data. As a result, the network is more likely to get stuck at a local minimum.

For non-end-to-end training methods like ACE and GLACE, the difference is that we can easily shuffle pixels from all rendered images and query images because the supervision relies only on the camera intrinsics and the planar coordinates of each pixel without further requirements of per-frame joint supervision.

Take GLACE as an example; our PoI could also be used as in Figure 2.(b); the difference is that the backbone should

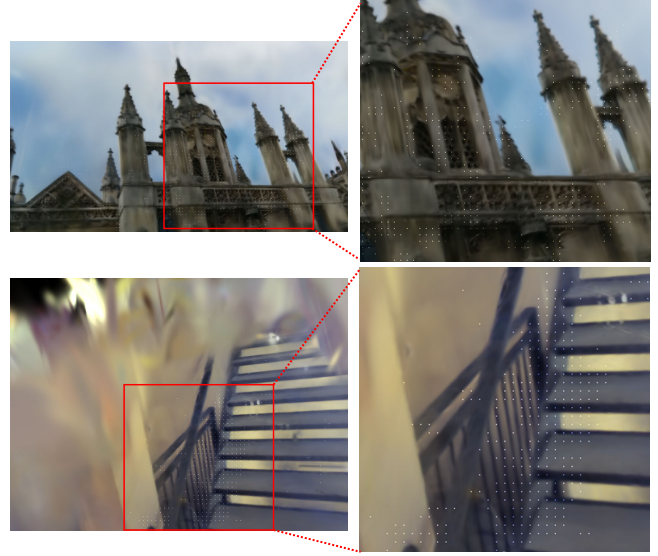


Figure 3: An example of the results of PoI in dataset 7Scenes and Cambridge Landmarks. To highlight the determined pixels of interest, we scale up the ‘Value’ (V) of the HSV representation of the images.

be replaced. We use the global encoder of GLACE to extract the same dimension of global features as the ACE features. We add the global feature and the ACE feature together and get the target feature maps. The following procedure remains unchanged.

3.5 Sparse input

Sparse input visual localization is a challenging task since both CPR and SCR are not good at estimating unseen parts of the scene because the regression models are trained only from RGB with weak geometric constraints. However, with the help of sparse input NVS, we would be able to extend the training views.

In this case, the challenge is that rendered frames from sparse-view NVS are generally of lower quality compared with those from dense-input NVS. The ratio between the input views and the NVS views is also reduced. If we still use the raw PoI method, the implicit neural map will be mainly contributed by rendered pixels. The accuracy will be influenced. To address this problem, we propose a coarse-to-fine training approach as shown in Figure 4. In the coarse stage, we use the same setting as in PoI; the only difference is that all training data are rendered images. So, the filter is applied to all rendered pixels, which we call the self-pruning step. In this step, in order to retain adequate pixels for training, we raise the filter’s threshold (for reprojection errors). We get a coarse model after self-pruning training. In the refinement stage, we fine-tuned the mapping model using real data and the remaining rendered data; we set the learning rate to lower than that of the coarse stage throughout the fine-tuning process. In this step, all pixels are put into the model without filtering.

We finally get the fine-tuned model and experiment on both

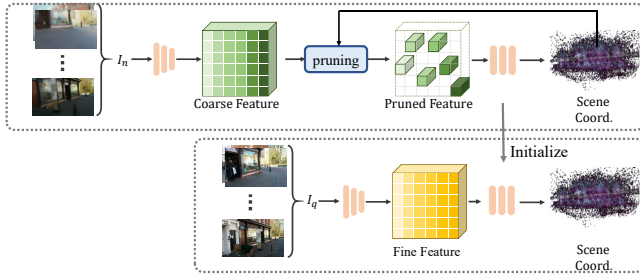


Figure 4: Pipeline of the coarse-to-fine strategy for sparse input localization.

indoor and outdoor datasets. The results and implementation details can be found in chapter 4.3.

4 Experiment

4.1 Implementation details

Dataset We evaluate the performance of our approaches on two public datasets, Microsoft 7Scenes Shotton *et al.* [2013] (**with SfM Pseudo GT**) and Cambridge Landmarks Kendall *et al.* [2015]. Our network takes RGB images and the camera extrinsic as input without using the depth information from the 7Scenes dataset or the reconstruction information from the Cambridge Landmarks dataset. We take the original resolution for the RGB images to make an accurate pose estimation.

To save time and computing resources, we do pose sampling and synthesis of new views offline and save the sampled camera poses and the rendered images on disk. During training time, we load rendered images along with the training set from the disk. For the scene ‘kitchen’ only, we split the training data into two clusters using the camera poses. We follow the rule of poker (a variant of ACE) and train two models with the clusters. During the evaluation, we choose the estimated pose from the model with a more significant number of inlier pixels of the Ransac algorithm. We use 1 NVIDIA V100 GPU for PoI training; for GLPoI, we use 4 V100 with distributed data-parallel training.

4.2 Localization results

The comparison of median translation and rotation errors between our proposed methods with different camera pose regression methods (top), scene coordinate regression methods (middle), and neural render pose estimation methods (bottom) in dataset 7Scenes is shown in Table 1. Generally speaking, scene coordinate regression methods outperform absolute camera pose regression methods in both translations and orientations. Unlike Zeller [2024], we include DFNet and LENS in NRP, although they use offline NVS. Our proposed method outperforms DSAC* and ACE by exploiting the additional information from the rendered novel views. Our ‘GLPoI’ beats ‘GLACE’ and achieves the state of the art.

The results of the Cambridge Landmarks datasets are shown in Table 2. Since apparent gaps exist between scene coordinate regression methods and absolute camera pose regression methods, we only list the results of SCR and NRP



Figure 5: The rendering views obtained based on pose estimations using different localization methods.

methods. We come to a similar conclusion as that of 7Scenes. Although we use additional rendered data, it can achieve training efficiency comparable to ACE. In order to intuitively compare the localization effects of different methods, we also used NVS to render the images corresponding to the poses estimated by different localization methods, as shown in Figure 5. The upper right is the original image, and the lower left is the image rendered using poses estimated using different methods.

4.3 Coarse-to-fine experiments of sparse input

To further evaluate the effectiveness of our method, we do an additional experiment with sparse input as mentioned in Chapter 3.5.

implement details: We use pre-trained MVSplatChen *et al.* [2024b] as the sparse NVS model. For datasets like 7Scenes, it takes thousands of images to train a small indoor scene with a scale of only several meters. To simulate the sparse input, we uniformly re-sample from the input data every 50 frames. For Scene ‘heads’, we keep only 20 frames. For outdoor datasets like Cambridge Landmarks, we split the data into multiple clusters according to the ground truth translations of camera pose (4 in the experiment) and used only one cluster for training.

The numerical results are shown in Table 3, **case ‘base’** denotes the sparse input circumstances with the baseline model. **Case ‘coarse’** is the self-pruning step of our method only using rendered data; we still use grid sampling as the novel pose sampling method. **Case ‘c2f’** denotes the fine-tuned results of our proposed method.

Based on the results, we may find that our fine-tuned model can achieve acceptable results with limited input compared to those that use all the training data.

4.4 Ablation of PoI

To evaluate the effectiveness of our PoI approach, we conducted some experiments on PoI in different settings. As shown in Table 4, we set the training process using only query data from the training set as the **case ‘base’**. In this case,

Table 1: Median errors of camera pose regression methods and scene coordinate regression methods on the 7Scenes dataset Shotton *et al.* [2013]. We **bold** the best results.

	Method	Scenes							Avg. (cm/ $^{\circ}$)
		Chess	Fire	Heads	Office	Pumpkin	Kitchen	Stairs	
CPR	PoseNet15	10/4.02	27/10.0	18/13.0	17/5.97	19/4.67	22/5.91	35/10.5	21/7.74
	Marepo	1.9/0.83	2.3/0.92	2.1/1.24	2.9/0.93	2.5/0.88	2.9/0.98	5.9/1.48	2.9/1.04
SCR	DSAC*	0.5 /0.17	0.8/0.28	0.5/0.34	1.2/0.34	1.2/0.28	0.7/0.21	2.7/0.78	1.1/0.34
	ACE	0.5 /0.18	0.8/0.33	0.5/0.33	1.0/0.29	1.0/0.22	0.8/0.2	2.9/0.81	1.1/0.34
NRP	GLACE	0.6/0.18	0.9/0.34	0.6/0.34	1.1/0.29	0.9/0.23	0.8/0.20	3.2/0.93	1.2/0.36
	LENS	3/1.30	10/3.70	7/5.80	7/1.90	8/2.20	9/2.20	14/3.60	8/3.00
	DFNet	3/1.12	6/2.30	4/2.29	6/1.54	7/1.92	7/1.74	12/2.63	6/1.93
	GSplatLoc	0.43/0.16	1.03/0.32	1.06/0.62	1.85/0.4	1.8/0.35	2.71/0.55	8.83/2.34	2.53/0.68
	Pol(ours)	0.5 / 0.15	0.7 / 0.31	0.6 / 0.30	0.9 / 0.26	1.0 / 0.20	0.7/0.22	2.4 / 0.70	1.0 / 0.31
	GLPoI(ours)	0.6/0.19	0.8/0.33	0.5 /0.33	0.9 /0.29	0.8 /0.22	0.6 / 0.19	2.8/0.77	1.0 /0.33

Table 2: Results on Cambridge Landmarks, because of the obvious gap between SCR-based methods and CPR-based methods, we only list SCR-based methods. column ‘Mapping time’ shows the training time of these methods (the GS model can be trained offline, and the training time of the GS model is less than PoI), and column ‘Mapping size’ is the memory consumption for saving the parameters of the network. We **bold** the best result for group ‘SCR’ and group ‘SCR w/ glob’ separately.

	Method	Mapping with Depth/Mesh	Mapping Time	Map Size	Scenes					Avg. (cm/ $^{\circ}$)
					King’s	Hospital	Shop	Church	Court	
SCR	SANet Yang <i>et al.</i> [2019]	Yes	1min	260M	32/0.5	32/0.5	10/0.5	16/0.6	328/2	84/0.8
	SRC Dong <i>et al.</i> [2022]	Yes	2min	40M	39/0.7	38/0.5	19/1	31/1.0	81/0.5	42/0.7
	DSAC* Brachmann and Rother [2021]	No	15h	28M	18 / 0.3	21/0.4	5/0.3	15/0.6	34/0.2	19/0.4
	Poker Brachmann <i>et al.</i> [2023]	No	20min	16M	18/0.3	25/0.5	5/0.3	9/0.3	28/0.1	17 / 0.3
	EGFS Liu <i>et al.</i> [2025]	No	21min	9M	14 / 0.3	28 / 0.1	19/0.4	5 / 0.2	10 /0.3	15 / 0.3
	GLACE Wang <i>et al.</i> [2024]	No	20min	13M	19 / 0.3	17/0.4	4 / 0.2	9/0.3	19/0.1	14 / 0.3
NRP	LENS Moreau <i>et al.</i> [2022b]	No	-	-	33/0.5	44/0.9	27/1.6	53/1.6	-	-
	GSplatLoc Zeller [2024]	No	-	-	27/0.46	20/0.71	5/0.36	16/0.61	-	-
	PoI (ours)	No	25min	16M	18 / 0.3	23/0.5	5 / 0.2	9/0.3	27/ 0.1	16 / 0.3
	GLPoI (ours)	No	25min	13M	19 / 0.3	16 /0.4	4 / 0.2	8/0.3	18/ 0.1	13 / 0.3

Table 3: Median errors of our proposed method with sparse input on 7Scenes and Cambridge dataset.

Method	7Scenes			Cambridge Landmarks		
	trans \downarrow	rot \downarrow	$U_{5cm,5^{\circ}}$ \uparrow	trans \downarrow	rot \downarrow	$U_{10cm,5^{\circ}}$ \uparrow
base	2.6cm	0.7 $^{\circ}$	68.9%	435cm	2.2 $^{\circ}$	15.7%
coarse	16.5cm	4.8 $^{\circ}$	11.2%	184cm	2.2 $^{\circ}$	15.8%
c2f	1.8cm	0.3$^{\circ}$	90.2%	26.9cm	0.3$^{\circ}$	20.4%

Table 4: Median errors of different implementations of PoI on 7Scenes and Cambridge dataset.

Method	7Scenes			Cambridge Landmarks		
	trans \downarrow	rot \downarrow	$U_{5cm,5^{\circ}}$ \uparrow	trans \downarrow	rot \downarrow	$U_{10cm,5^{\circ}}$ \uparrow
base	1.1cm	0.3$^{\circ}$	97.1%	17.7cm	0.3$^{\circ}$	32.4%
base+poa	2.3cm	1.58 $^{\circ}$	89.6%	17.6cm	0.3$^{\circ}$	32.2%
base+por	1.4cm	0.46 $^{\circ}$	95.9%	18.0cm	0.3$^{\circ}$	30.4%
base+poi	1.0cm	0.3$^{\circ}$	98.9%	16.4cm	0.3$^{\circ}$	33.1%

the training setting is similar to ACE’s. **Case ‘base+por’** indicates the training with data from the training set and all rendered pixels of the proposed novel pose rendering method.

Case ‘base+por’ denotes the pixel-of-random method, which uses randomly sampled pixels from the NVS, and all else are the same with case ‘base+poi’. **Case ‘base+poi’** is our final method. From the results, we may find that if we directly use sampled images and the training data without filtering, the results will be worse than the baseline (7scenes). It is easy to understand that because the mapping process is filled with low-quality pixels, it would misguide the network. If we randomly sample some pixels, we still won’t get a good estimate.

5 Conclusion

In this paper, we propose a pixel of interest filter for scene coordinate regression. The filter is designed for non-end-to-end methods, which enjoy good converging speed. With the filter, we also designed a coarse-to-fine pipeline for sparse input scenarios. We conducted experiments on indoor and outdoor datasets and achieved state-of-the-art camera pose estimation with comparable training time.

References

Eduardo Arnold, Jamie Wynn, Sara Vicente, Guillermo Garcia-Hernando, Áron Monszpart, Victor Prisacariu,

- Daniyar Turmukhambetov, and Eric Brachmann. Map-free visual relocalization: Metric pose relative to a single image. In *Proceedings of the European Conference on Computer Vision*, pages 690–708. Springer, 2022.
- Eric Brachmann and Carsten Rother. Learning less is more: 6d camera localization via 3d surface regression. In *Proceedings of the IEEE Conference on Computer Vision and Pattern Recognition*, pages 4654–4662, 2018.
- Eric Brachmann and Carsten Rother. Expert sample consensus applied to camera re-localization. In *Proceedings of the IEEE/CVF International Conference on Computer Vision*, pages 7525–7534, 2019.
- Eric Brachmann and Carsten Rother. Visual camera re-localization from rgb and rgb-d images using dsac. *IEEE transactions on pattern analysis and machine intelligence*, 44(9):5847–5865, 2021.
- Eric Brachmann, Frank Michel, Alexander Krull, Michael Ying Yang, Stefan Gumhold, et al. Uncertainty-driven 6d pose estimation of objects and scenes from a single rgb image. In *Proceedings of the IEEE conference on computer vision and pattern recognition*, pages 3364–3372, 2016.
- Eric Brachmann, Alexander Krull, Sebastian Nowozin, Jamie Shotton, Frank Michel, Stefan Gumhold, and Carsten Rother. Dsac-differentiable ransac for camera localization. In *Proceedings of the IEEE conference on computer vision and pattern recognition*, pages 6684–6692, 2017.
- Eric Brachmann, Tommaso Cavallari, and Victor Adrian Prisacariu. Accelerated coordinate encoding: Learning to relocalize in minutes using rgb and poses. In *Proceedings of the IEEE/CVF Conference on Computer Vision and Pattern Recognition*, pages 5044–5053, 2023.
- Samarth Brahmbhatt, Jinwei Gu, Kihwan Kim, James Hays, and Jan Kautz. Geometry-aware learning of maps for camera localization. In *Proceedings of the IEEE Conference on Computer Vision and Pattern Recognition*, pages 2616–2625, 2018.
- Shuai Chen, Zirui Wang, and Victor Prisacariu. Directposenet: absolute pose regression with photometric consistency. In *2021 International Conference on 3D Vision (3DV)*, pages 1175–1185. IEEE, 2021.
- Shuai Chen, Xinghui Li, Zirui Wang, and Victor A Prisacariu. Dfnet: Enhance absolute pose regression with direct feature matching. In *Computer Vision–ECCV 2022: 17th European Conference, Tel Aviv, Israel, October 23–27, 2022, Proceedings, Part X*, pages 1–17. Springer, 2022.
- Shuai Chen, Tommaso Cavallari, Victor Adrian Prisacariu, and Eric Brachmann. Map-relative pose regression for visual re-localization. In *Proceedings of the IEEE/CVF Conference on Computer Vision and Pattern Recognition*, pages 20665–20674, 2024.
- Yuedong Chen, Haofei Xu, Chuanxia Zheng, Bohan Zhuang, Marc Pollefeys, Andreas Geiger, Tat-Jen Cham, and Jianfei Cai. Mvsplat: Efficient 3d gaussian splatting from sparse multi-view images. *arXiv preprint arXiv:2403.14627*, 2024.
- Angela Dai, Matthias Nießner, Michael Zollhöfer, Shahram Izadi, and Christian Theobalt. Bundlefusion: Real-time globally consistent 3d reconstruction using on-the-fly surface reintegration. *ACM Transactions on Graphics (ToG)*, 36(4):1, 2017.
- Siyan Dong, Shuzhe Wang, Yixin Zhuang, Juho Kannala, Marc Pollefeys, and Baoquan Chen. Visual localization via few-shot scene region classification. In *2022 International Conference on 3D Vision (3DV)*, pages 393–402. IEEE, 2022.
- Hanjiang Hu, Zhijian Qiao, Ming Cheng, Zhe Liu, and Hesheng Wang. Dasgil: Domain adaptation for semantic and geometric-aware image-based localization. *IEEE Transactions on Image Processing*, 30:1342–1353, 2020.
- Shahram Izadi, David Kim, Otmar Hilliges, David Molyneaux, Richard Newcombe, Pushmeet Kohli, Jamie Shotton, Steve Hodges, Dustin Freeman, Andrew Davison, et al. Kinectfusion: real-time 3d reconstruction and interaction using a moving depth camera. In *Proceedings of the 24th annual ACM symposium on User interface software and technology*, pages 559–568, 2011.
- Alex Kendall, Matthew Grimes, and Roberto Cipolla. Posenet: A convolutional network for real-time 6-dof camera relocalization. In *Proceedings of the IEEE international conference on computer vision*, pages 2938–2946, 2015.
- Bernhard Kerbl, Georgios Kopanas, Thomas Leimkühler, and George Drettakis. 3d gaussian splatting for real-time radiance field rendering. *ACM Trans. Graph.*, 42(4):139–1, 2023.
- Jonas Kulhanek, Songyou Peng, Zuzana Kukelova, Marc Pollefeys, and Torsten Sattler. Wildgaussians: 3d gaussian splatting in the wild. *arXiv preprint arXiv:2407.08447*, 2024.
- Xiaotian Li, Juha Ylioinas, Jakob Verbeek, and Juho Kannala. Scene coordinate regression with angle-based reprojection loss for camera relocalization. In *Proceedings of the European Conference on Computer Vision Workshops*, pages 0–0, 2018.
- Ting-Ru Liu, Hsuan-Kung Yang, Jou-Min Liu, Chun-Wei Huang, Tsung-Chih Chiang, Quan Kong, Norimasa Kobori, and Chun-Yi Lee. Reprojection errors as prompts for efficient scene coordinate regression. In *European Conference on Computer Vision*, pages 286–302. Springer, 2025.
- Ricardo Martin-Brualla, Noha Radwan, Mehdi SM Sajjadi, Jonathan T Barron, Alexey Dosovitskiy, and Daniel Duckworth. Nerf in the wild: Neural radiance fields for unconstrained photo collections. In *Proceedings of the IEEE/CVF Conference on Computer Vision and Pattern Recognition*, pages 7210–7219, 2021.
- Daniela Massiceti, Alexander Krull, Eric Brachmann, Carsten Rother, and Philip HS Torr. Random forests versus neural networks—what’s best for camera localization? In *2017 IEEE international conference on robotics and automation (ICRA)*, pages 5118–5125. IEEE, 2017.

- Iaroslav Melekhov, Juha Ylioinas, Juho Kannala, and Esa Rahtu. Image-based localization using hourglass networks. In *Proceedings of the IEEE international conference on computer vision workshops*, pages 879–886, 2017.
- Ben Mildenhall, Pratul P Srinivasan, Matthew Tancik, Jonathan T Barron, Ravi Ramamoorthi, and Ren Ng. Nerf: Representing scenes as neural radiance fields for view synthesis. *Communications of the ACM*, 65(1):99–106, 2021.
- Arthur Moreau, Nathan Piasco, Dzmitry Tsishkou, Bogdan Stanciulescu, and Arnaud de La Fortelle. Coordinet: uncertainty-aware pose regressor for reliable vehicle localization. In *Proceedings of the IEEE/CVF Winter Conference on Applications of Computer Vision*, pages 2229–2238, 2022.
- Arthur Moreau, Nathan Piasco, Dzmitry Tsishkou, Bogdan Stanciulescu, and Arnaud de La Fortelle. Lens: Localization enhanced by nerf synthesis. In *Conference on Robot Learning*, pages 1347–1356. PMLR, 2022.
- Raul Mur-Artal, Jose Maria Martinez Montiel, and Juan D Tardos. Orb-slam: a versatile and accurate monocular slam system. *IEEE transactions on robotics*, 31(5):1147–1163, 2015.
- Tony Ng, Adrian Lopez-Rodriguez, Vassileios Balntas, and Krystian Mikolajczyk. Reassessing the limitations of cnn methods for camera pose regression. *arXiv preprint arXiv:2108.07260*, 2021.
- Pulak Purkait, Cheng Zhao, and Christopher Zach. Synthetic view generation for absolute pose regression and image synthesis. In *BMVC*, page 69, 2018.
- Noha Radwan, Abhinav Valada, and Wolfram Burgard. Vloc-net++: Deep multitask learning for semantic visual localization and odometry. *IEEE Robotics and Automation Letters*, 3(4):4407–4414, 2018.
- Yoli Shavit and Yosi Keller. Camera pose auto-encoders for improving pose regression. In *Proceedings of the European Conference on Computer Vision*, pages 140–157. Springer, 2022.
- Jamie Shotton, Ben Glocker, Christopher Zach, Shahram Izadi, Antonio Criminisi, and Andrew Fitzgibbon. Scene coordinate regression forests for camera relocalization in rgbd images. In *Proceedings of the IEEE Conference on Computer Vision and Pattern Recognition*, pages 2930–2937, 2013.
- Hajime Taira, Masatoshi Okutomi, Torsten Sattler, Mircea Cimpoi, Marc Pollefeys, Josef Sivic, Tomas Pajdla, and Akihiko Torii. Inloc: Indoor visual localization with dense matching and view synthesis. In *Proceedings of the IEEE Conference on Computer Vision and Pattern Recognition*, pages 7199–7209, 2018.
- Chengzhou Tang and Ping Tan. Ba-net: Dense bundle adjustment network. *arXiv preprint arXiv:1806.04807*, 2018.
- Julien Valentin, Matthias Nießner, Jamie Shotton, Andrew Fitzgibbon, Shahram Izadi, and Philip HS Torr. Exploiting uncertainty in regression forests for accurate camera relocalization. In *Proceedings of the IEEE conference on computer vision and pattern recognition*, pages 4400–4408, 2015.
- Bing Wang, Changhao Chen, Chris Xiaoxuan Lu, Peijun Zhao, Niki Trigoni, and Andrew Markham. Atloc: Attention guided camera localization. In *Proceedings of the AAAI Conference on Artificial Intelligence*, volume 34, pages 10393–10401, 2020.
- Fangjinhua Wang, Xudong Jiang, Silvano Galliani, Christoph Vogel, and Marc Pollefeys. Glace: Global local accelerated coordinate encoding. In *Proceedings of the IEEE/CVF Conference on Computer Vision and Pattern Recognition*, pages 21562–21571, 2024.
- Luwei Yang, Ziqian Bai, Chengzhou Tang, Honghua Li, Yasutaka Furukawa, and Ping Tan. Sanet: Scene agnostic network for camera localization. In *Proceedings of the IEEE/CVF international conference on computer vision*, pages 42–51, 2019.
- Lin Yen-Chen, Pete Florence, Jonathan T Barron, Alberto Rodriguez, Phillip Isola, and Tsung-Yi Lin. inerf: Inverting neural radiance fields for pose estimation. In *2021 IEEE/RSJ International Conference on Intelligent Robots and Systems (IROS)*, pages 1323–1330. IEEE, 2021.
- Atticus J Zeller. Gsplatloc: Ultra-precise camera localization via 3d gaussian splatting. *arXiv preprint arXiv:2412.20056*, 2024.

PoI: Pixel of Interest for Novel View Synthesis Assisted Scene Coordinate Regression

– Supplementary Materials –

Author Name

Affiliation

email@example.com

1 Visulized Results of sparse input



(a) Coarse stage results.

(b) Fine stage results.

Figure 1: The localization trajectories of the coarse-to-fine method for sparse view circumstances.

2 We construct the mesh based on the estimated scene co-
3 ordinates of the coarse stage and the fine stage and visualize
4 the camera pose estimation results in Figure 1. We may find
5 that in the coarse stage, the pose estimation error is relatively
6 large, and the quality of the reconstructed details is low. In
7 the refined stage, the performance is much better.

8 2 Visulized Results of PoI

9 The visualized results of the 7Scenes camera pose estima-
10 tion are shown in Figure 2. The trajectories of the ground
11 truth camera pose are drawn in white, while the color of the
12 predicted trajectories is set according to the estimated trans-
13 lation error. As translation errors increase, the color tends
14 to change from purple to red, following the color spectrum
15 of the rainbow. To make the camera pose prediction results
16 clearer, we also draw a mesh rendering view built from the
17 estimated scene coordinates of the training data in the same
18 frame for correspondence.

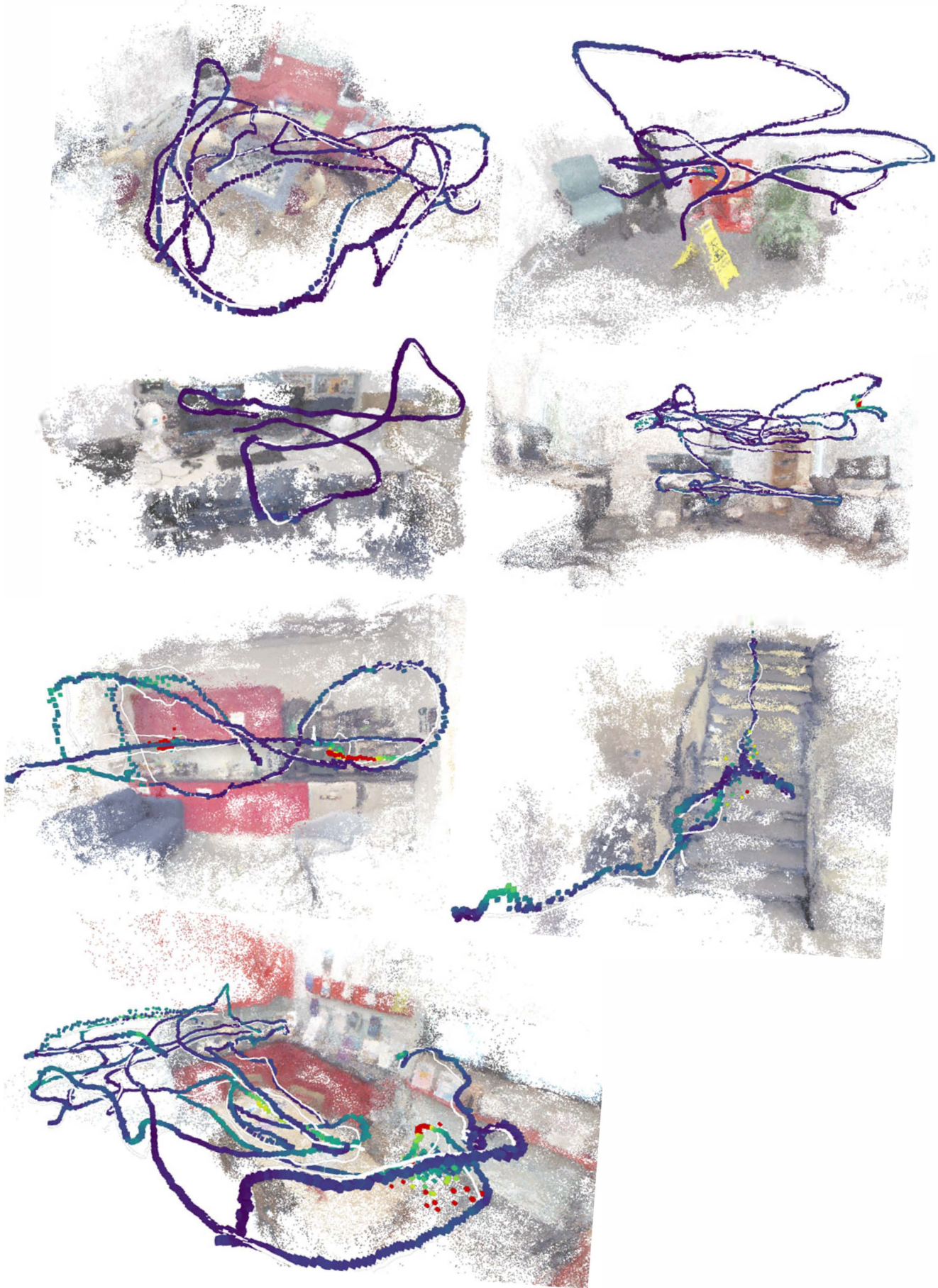


Figure 2: Visualized camera pose estimation results of 7scenes dataset.